Tailoring band gaps of insulators by adsorption at surface defects: Benzoic acids on NaCl surfaces

Wei Chen, Christoph Tegenkamp, and Herbert Pfnür*
Institut für Festkörperphysik, Leibniz Universität Hannover, 30167 Hannover, Germany

Thomas Bredow
Institut für Physikalische und Theoretische Chemie, Universität Bonn, 53115 Bonn, Germany
(Received 9 February 2009; revised manuscript received 20 May 2009; published 17 June 2009)

The adsorption of benzoic acid and its OH-substituted derivatives, namely, salicylic acid (SA) and *para*-salicylic acid on various NaCl surfaces has been investigated by density-functional theory with hybrid exchange-correlation functional. The ideal NaCl(100) surface is chemically inert as evidenced by the low binding energies. The molecular adsorption can be enhanced by both an anion vacancy and a surface step site. The bonding between the surface Na and the carboxylic O atom is of covalent character for all adsorption geometries. Our calculations show that the adsorption of SA has the largest binding energy of all three acids due to the additional interaction between Na and the phenolic O atom. Charge transfer between the molecule and the surface is generally very small, except in the presence of an anion vacancy where the unpaired electron is mostly transferred to the adsorbate. Surface defects generally have a strong influence on the electronic structure of the adsorbed molecules. Specifically, the adsorption of SA at [011]-oriented steps can significantly reduce the effective band gap to 1.6 eV due to the up shift of the Cl 3*p* levels at the undercoordinated step edge. Implications of these results to the contact charging effect between wide-band-gap insulators will be discussed.

DOI: 10.1103/PhysRevB.79.235419 PACS number(s): 68.43.Bc, 71.15.Mb, 73.20.Hb

I. INTRODUCTION

Sodium chloride (NaCl), as a prototype of a wide-band-gap insulator, is one of the most common compounds in nature. Its bulk properties have been studied extensively in the past,[1] while for the surface the progress was hampered since some popular surface-sensitive techniques cannot be directly applied to ionic materials because of surface charging. The problem, however, has been circumvented by the epitaxial growth of thin films on metallic substrates.[2,3] Usually perfect surfaces of wide-band-gap insulators are quite inert. Therefore they are often used as support for chemical and technical applications.

Organic thin films, specifically conjugated polymers, have recently been the subject of worldwide research effort for their exciting applications in organic light-emitting diodes (OLEDs), photovoltaics, and organic field-effect transistors (OFETs).[4–8] One of the most appealing aspects of conjugated molecules is that their highest occupied molecular orbital (HOMO)-lowest unoccupied molecular orbital (LUMO) gaps can be tuned easily by adding specific functional groups to the molecules, which makes the electronic conductivity variable over several orders of magnitude by substitution.[9] This unique property also provides a new possibility for tailoring the band gap of insulators.[10,11] It turns out that adsorption of organic molecules on perfect insulating surface can reduce the effective band gap to the HOMO-LUMO separation of the adsorbate. In fact, this is also implied by the electrostatic separation process of insulating materials, making use of the contact charging effect. It has been observed that the addition of certain organic molecules such as salicylic acid (SA) can separate NaCl and KCl in salt mines efficiently.[12] However such successful separation cannot be achieved by mixing with some other molecules such as benzoic acid (BA) or *para*-salicylic acid (*p*-SA). This selectivity suggests that the molecule plays an important role in the electronic properties of the adsorbed system.

Although contact charging is a common phenomenon of insulators, the detailed microscopic mechanism is still lacking. In fact, it is obvious that the surfaces of NaCl or KCl grains used for separation can never be free of defects. Even on pristine NaCl(100) surface, monatomic steps and kinks are also present inevitably. Indeed defects (vacancies, steps, etc.) are often decisive in chemical reactivity on insulator surfaces,[13–15] and they play an important role in both the adsorption geometry and the electronic structure. For example, a few experiments and theoretical studies suggest dissociative adsorption of water on NaCl(100) in the presence of F_s center.[14,16,17] Malaske *et al.* studied the adsorption of SA on the perfect NaCl(100) surface and at surface color centers (F_s) with electron energy loss spectroscopy (EELS) and UV photoelectron spectroscopy (UPS).[10] It was found the binding of SA at the F_s center is much stronger than on undistorted surfaces. The adsorption of SA also introduces unoccupied states in the forbidden gap of the NaCl surface, and thus the effective band gap can be lowered. However, atomistic models for adsorption of conjugated molecules on NaCl surface are not available yet. Indeed only a few theoretical adsorption studies on NaCl have been made within the last decade and most of them were dedicated to some simple adsorbates such as water and H_2.[14,17–21] Consequently the microscopic picture of the interaction between these organic molecules and NaCl surface is not clear. Neither is the origin of contact charging between NaCl and KCl.

The aim of this work is to investigate the adsorption of simple and typical conjugated molecules, namely, BA, SA,

and *p*-SA on NaCl(100) surfaces and to understand the influence of surface defects on the adsorption process and on the electronic properties with the help of density-functional theory (DFT). Specifically the adsorption at the ideal NaCl(100) surface, at the surface F_s center and at two types of step sites will be discussed in this work. These results could help us for a better understanding of the interaction between conjugated molecules and wide-band-gap ionic surfaces and could also provide insights into the band-gap tailoring of wide-band-gap insulators.

II. COMPUTATIONAL DETAILS

Periodic DFT calculations were performed with the CRYSTAL06 code[22] with the PW1PW hybrid exchange-correlation functional.[23] The PW1PW hybrid functional mixes 80% of the Perdew-Wang 91 (PW91) generalized gradient approximation (GGA) exchange[24] with 20% of the exact Hartree-Fock (HF) exchange and describes correlation with the PW91 correlation functional.[23] In an earlier study of MgO, NiO, and CoO, it was found that the PW1PW functional gives a better description of structural and electronic properties than other hybrid functionals.[23] An important aspect of the hybrid functional is that the predicted band gap can be much more accurate than GGA and HF, which is crucial for the determination of defect states and the alignment of unoccupied states from organic molecules in the band gap. In DFT, the exchange-correlation energy is evaluated via numerical integration, which employs a grid of points in space. A large grid, namely, pruned (75,434) grid, was adopted in this study for high accuracy energy calculations and geometry optimizations.[22]

The atomic wave function in CRYSTAL06 was constructed as a Slater determinant of Bloch functions which are chosen as linear combination of Gaussian-type functions (GTFs). For Na and Cl, 8-511 and 86-311 G split-valence basis sets were adopted in the present study, respectively.[25] Regarding the isolated Na^+ and Cl^- for the lattice energy calculation, reoptimized exponents of two most diffuse *sp* shells were used for a better description of the valence tails.[25] In the calculation of the energy of the isolated Cl atom, the exponent of the most diffuse shell was also optimized (0.117 $bohr^{-2}$). C, O, and H atoms of the organic molecules were expanded by Pople-type 6-31G(*d*) basis sets. A test calculation with larger 6-311G(*d*,*p*) basis sets on C, O, and H atoms yields an adsorption energy difference of only 0.04 eV to respect to 6-31G(*d*) basis sets for the SA adsorbed on NaCl(100). This suggests that the quality of 6-31G(*d*) is satisfactory for describing the interaction between benzoic acids and NaCl.

The cell parameters of bulk NaCl have been fully optimized using the Broyden-Fletcher-Goldfarb-Shanno (BFGS) algorithm.[22] A fine Monkhorst-Pack *k*-point mesh of $8\times8\times8$ was employed, corresponding to 29 *k* points in the irreducible Brillouin zone (IBZ) of the primitive unit cell. The energy convergence criteria for self-consistent field (SCF) calculation was 10^{-7} hartree. Geometry optimizations were considered as converged when the residual force was below 0.0003 hartree/bohr. The optimized cell parameters were used for further surface and adsorption calculations.

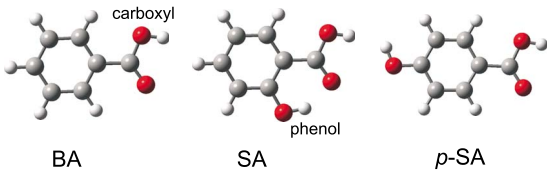

FIG. 1. (Color online) Structures of benzoic, salicylic, and parasalicylic acids. The red (black), gray, and small white atom represent oxygen, carbon, and hydrogen, respectively.

The surface was modeled with two-dimensional slabs, and no periodicity along the direction normal to the surface was imposed. For adsorption studies on perfect NaCl(100), we used two-sided adsorption on a (3×3) supercell with five-layer-thick slab (90 atoms). A neutral surface anion vacancy (F_s^0) was created by manually removing one Cl atom in the top layer. Auxiliary basis functions have been imposed at the center of the vacancy to yield an accurate description of the unpaired electron. A spin-polarized DFT calculation is therefore required for the F_s center.

The [001]-oriented steps were modeled by simply using the NaCl(301) vicinal surface with monatomic (001) steps separated by (100) terraces with a width of three anion-cation interatomic distances, whereas the [011]-oriented steps were constructed from a four-layer NaCl(100) slab whose step edges of the first layer were cleaved along the $\langle 0\bar{1}1\rangle$ direction. The choices of the stepped surface models represent a compromise between moderate sizes of unit cells and reasonable computational costs. During geometry relaxation, all atoms were allowed to move except for the [011]-oriented step, where the bottom layer was kept fixed. For all the adsorption calculations, we used a *k*-point mesh of 4×4 which corresponds to ten *k* points in the IBZ of the slab. The thresholds controlling the truncation criteria for the calculation of Coulomb and exchange integrals were set to 1×10^{-7} (cutoff parameters ITOL1 to ITOL4) and 1×10^{-8} (ITOL5).[22]

III. ADSORPTION ON THE IDEAL NaCl(100) SURFACE

A. Gas phases BA, SA, and *p*-SA

First the ground-state geometries and energetics of these three isolated organic molecules were investigated. Their molecular structures are shown in Fig. 1. All molecules are flat due to sp^2 hybridization over the benzene, carboxylic, and phenolic groups. The values for the intramolecular bond lengths are given in Table I and show good agreement with earlier experimental reports.

In order to identify the electronic structure difference between benzoic acid and various hydroxybenzoic acids, the frontier orbitals, including LUMO and HOMO to HOMO -3 were computed, which are presented in Table I. These results have been compared to the occupied electronic states of condensed films of these acids resolved by UPS.[28] For all benzoic acids, the HOMO and the HOMO-1 are primarily the bonding states of the cyclic benzene ring. However, the presence of phenolic OH group in SA and *p*-SA changes the

TABLE I. Intramolecular bond lengths and molecular orbital energies of benzoic acid, salicylic acid and *para*salicylic acid. The C-C is the average values of the six bond lengths between neighboring carbon atoms over the aromatic ring. The molecular orbital energies are shifted so that the HOMO energy is zero.

	BA		SA		*p*-SA	
	PW1PW	Expt.[a]	PW1PW	Expt.[b]	PW1PW	
Bond lengths (Å)						
C-C	1.394	1.388	1.399	1.385	1.395	
C-C_{carb}	1.482	1.484	1.460	1.457	1.475	
C_{carb}-O_{carb}	1.351		1.341	1.307	1.353	
C_{carb}=O_{carb}	1.213		1.231	1.234	1.214	
O_{carb}-H	0.974		0.974	1.000	0.973	
C-O_{phenol}			1.336	1.358	1.354	
O_{phenol}-H			0.990	1.029	0.968	
	PW1PW	Expt.[c]	PW1PW	Expt.[c]	PW1PW	Expt.[c]
Orbital energies (eV)						
LUMO	5.81		4.79		5.36	
HOMO	0.00	0.00	0.00	0.00	0.00	0.00
HOMO−1	−0.05	−0.18	−1.04	−1.00	−0.81	−0.73
HOMO−2	−0.37		−1.67		−0.97	
HOMO−3	−1.55	−2.36	−2.82	−3.10	−2.10	−2.58

[a]Reference 26.
[b]Reference 27.
[c]Reference 28.

intramolecular interaction and leads to a larger separation between HOMO and HOMO−1 than that of BA. For BA, HOMO and HOMO−1 are almost degenerate, which is very similar to the benzene molecule. In addition, we found that SA has the smallest HOMO-LOMO gap among all three acids, whereas the gap for *p*-SA is the largest. A detailed description of the molecular orbitals of hydroxybenzoic acids can be found in our earlier publication.[28]

B. Bulk NaCl

We briefly examined the bulk properties of NaCl as a starting point for further adsorption studies. The NaCl crystal structure is a face-centered cubic (space group $Fm\bar{3}m$). The equilibrium lattice constant (a_0), bulk modulus (B_0), and lattice energy (E_l) were calculated and compared to experiment, which are given in Table I. The lattice constant and bulk modulus were calculated with several methods, including HF and GGA with functional PW91 and two hybrid functionals, namely, Becke's three-parameter exchange functional and the Lee-Yang-Parr correlation functional (B3LYP) (Ref. 29) and PW1PW. It was found that the lattice constant predicted by PW1PW (5.68 Å) is closest to experiment with a slight overestimation of 0.7%. The bulk modulus was obtained by fitting the curve $E(V)$ with a strain (ϵ) matrix. PW1PW gives a more accurate description of the bulk modulus although the value is underestimated by 6.0%. The lattice energy (E_l) of NaCl at 0 K is defined as in Eq. (1) as follows:

$$E_l = E_{\mathrm{NaCl}} - E_{\mathrm{Na}^+} - E_{\mathrm{Cl}^-}, \tag{1}$$

where E_{NaCl}, E_{Na^+}, and E_{Cl^-} refer to the total energy of bulk NaCl, isolated Na, and Cl ions, respectively. It can be seen that although all methods are able to obtain reasonable lattice energies; E_l calculated by PW1PW (8.00 eV) is closest to the experimental value.

NaCl is a direct band-gap insulator, as is shown in the band structure in Fig. 2(a). In Table II, the band-gap values computed with HF and several DFT functionals are reported. It is not surprising that the band gap obtained with HF or the pure GGA functional is either far too wide or too narrow. Hybrid functionals are able to improve the band-gap value, although it is still somehow underestimated. In particular, PW1PW yielded a band gap of 7.15 eV for bulk NaCl, which is in better agreement with experiment than B3LYP. The density of states (DOS) plotted in Fig. 2(b) gives some insights into the electronic structure. The NaCl valence band is essentially formed by *p* states of Cl atom, whereas the conduction band mainly consists of Cl *s* and *p* states. The *s* states of Na have only marginal contribution to the conduction band. While this is on the contrary to common belief that the conduction band of NaCl consists of Na *s* state solely, recent calculations proved that the conduction band indeed has a predominant chlorine character.[33] From Fig. 2 it can be seen that the valence bandwidth is 1.97 eV, comparable to the experimental value of 1.8 eV. The small band dispersion is an indication of strong ionic bonding between Na and Cl

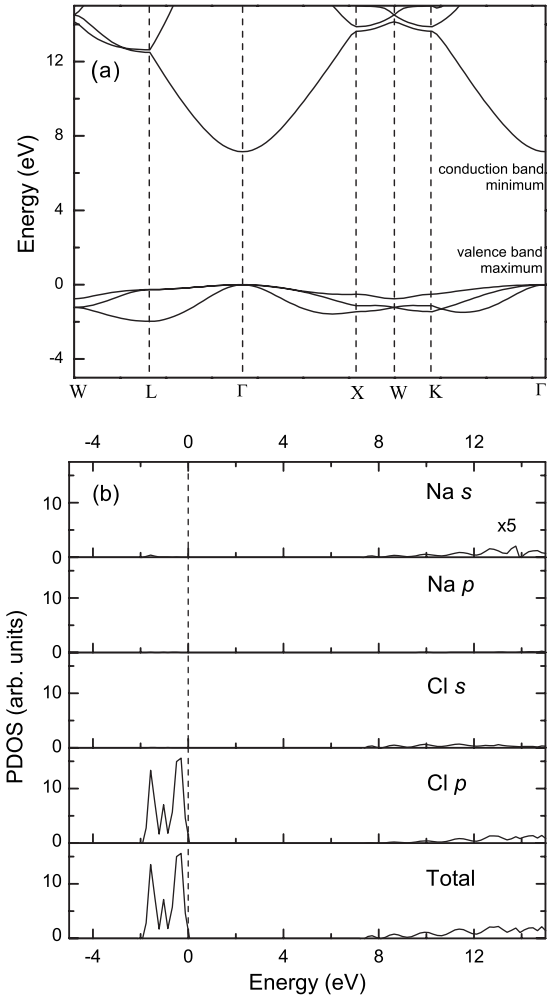

FIG. 2. (a) Band structure of bulk NaCl and (b) total DOS and projected density of states (PDOS) onto the *s* and the *p* states of Na and Cl. The top of the valence band was set to zero energy. All calculations were performed with the PW1PW hybrid functional.

atoms. The ionic nature can also be evidenced by a Mulliken population analysis, in which the net atomic charges of Na and Cl are $+0.972e$ and $-0.972e$, respectively.

C. NaCl(100) surface

We start the study of NaCl(100) surface with the surface energy calculation because it is the most basic thermodynamic quantity of a surface which can be used to validate the theoretical method and model. The surface energy can be expressed as[34]

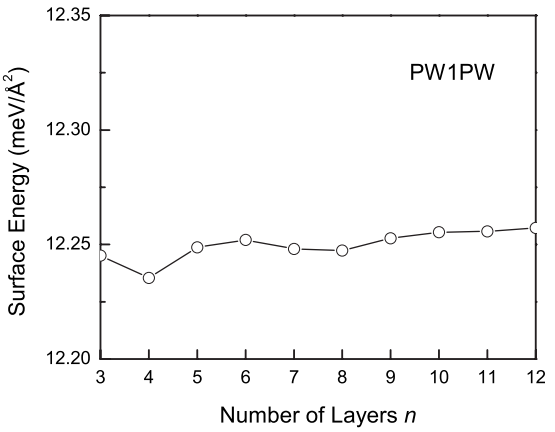

FIG. 3. Surface energy of NaCl(100) calculated for various numbers of layers.

$$\gamma = \lim_{n\to\infty} E_s(n) = \lim_{n\to\infty} \frac{E(n) - n[E(n) - E(n-1)]}{2A}, \qquad (2)$$

where $E(n)$ is the total energy of an n-layer slab and A is the area of the primitive surface cell. The factor 2 accounts for the upper and the lower surfaces of the slab. Thus $E_s(n)$ is the energy per unit cell area needed to form the surface from the bulk, and it converges to the surface energy per unit area as more layers are added. In this study up to 12 layers have been used to check the surface energy convergence, as is illustrated in Fig. 3. The calculated γ is 12.25 meV/Å^2, consistent with the results obtained by other functionals and earlier experiments.[35] E_s shows a rapid convergence after three and more layers have been put together. In fact, the E_s difference between 5- and 12-layer slabs is only 0.08% of the γ value. The relaxation of NaCl(100) surface (see Table III) induces small vertical displacements of Na and Cl atoms in the first and second layers of the slab, whereas there is almost no change for atoms in deeper layers. The average rumpling of the surface is calculated with the following relation:

$$\Delta_i = \tfrac{1}{2}(\Delta_{z,\mathrm{Na}(i)} - \Delta_{z,\mathrm{Cl}(i)}), \qquad (3)$$

where $\Delta_{z,\mathrm{Na}(i)}$ and $\Delta_{z,\mathrm{Cl}(i)}$ are the vertical displacements of Na and Cl in the ith layer. It can be seen from the calculation

TABLE II. Calculated equilibrium lattice constant (a_0), bulk modulus (B_0), lattice energy (E_l), and band gap (E_g) of NaCl.

Parameters	HF	PW91	B3LYP	PW1PW	Expt.
a_0 (Å)	5.79	5.72	5.73	5.68	5.64[a]
B_0 (GPa)	22.9	24.2	24.9	25.0	26.6[b]
E_l (eV)	7.71	7.98	7.82	8.00	8.20[a]
E_g (eV)	14.00	5.40	7.00	7.15	8.5[c]

[a]Reference 30.
[b]Reference 31.
[c]Reference 32.

TABLE III. The relaxation of the NaCl(100) surface with 5- and 12-layer slabs. The subscripts 1, 2, and 3 designate the first, the second, and the third layers, respectively.

	Δz (Å)						Δ_i (Å)			Δ_{12} (%)	Δ_{23} (%)
	Na_1	Cl_1	Na_2	Cl_2	Na_3	Cl_3	1(Na-Cl)	2(Na-Cl)	3(Na-Cl)		
Five-layer slab	−0.023	0.019	0.002	−0.003	0.000	0.000	−0.021	0.003	0.000	−0.05	−0.02
12-layer slab	−0.023	0.020	0.003	−0.003	0.001	0.001	−0.022	0.003	0.000	−0.04	−0.03
Expt.[a]							−0.07	0.01	0.00	−1.4	0.1

[a]Reference 36.

that in the top layer the Na atom tends to move toward the bulk by 0.023 Å while the Cl atom relaxes away from the bulk by 0.020 Å. The buckling of the surface atoms was also found in a low-energy electron diffraction (LEED) experiment,[36] but the rumpling observed by LEED is larger. It is obvious that the buckling of surface atoms also affects the interlayer distance. The change in the interlayer distance $\Delta_{i,i+1}$ is defined as

$$\Delta_{i,i+1} = \frac{\Delta_{z,\mathrm{Na}(i)} + \Delta_{z,\mathrm{Cl}(i)} - \Delta_{z,\mathrm{Na}(i+1)} - \Delta_{z,\mathrm{Cl}(i+1)}}{a_0}, \qquad (4)$$

where a_0 is the equilibrium lattice constant of NaCl. According to both the calculation and the LEED the distance between the upper two layers is reduced after relaxation. Small buckling of atoms in the second and third layers leads to much smaller changes in the interlayer spacing between these two layers. In addition, the results obtained from the five-layer slab agree quite well to the 12-layer slab. Therefore we will use a five-layer supercell slab for the study of adsorption on perfect NaCl(100).

Before proceeding to the next section, we give a glimpse into the electronic structure of NaCl(100) surface. Figure 4(a) shows the band structure of NaCl(100) obtained from a relaxed five-layer slab. The unrelaxed (100) slab exhibits a very similar electronic structure because of the small relaxation and rumpling at the surface. The electronic structure of NaCl(100) surface is qualitatively identical to that of the bulk. The calculated surface band gaps are 7.41 and 7.20 eV obtained from the 5- and 12-layer slabs, respectively. This, however, is contradictory to the common belief that band gap of the ionic surface should be smaller than that of the bulk due to the decreased Madelung potential at the surface. For reference, we calculated the electronic structure of a thicker slab consisting of 30 layers of atoms and obtained a band gap of 7.15 eV, which is the same as the bulk value. This is in agreement with previous DFT calculations based on the plane-wave pseudopotential approach, where the band gaps for both the bulk and the (100) surface were found to be identical.[35] Finally, the layer-resolved DOS of a five-layer slab is given in Fig. 4(b). One can see the narrowing of the valence bandwidth in the first layer, as well as a small shift of the peaks to the valence-band maximum (VBM). The second and third layers, however, already exhibit bulklike electronic properties.

D. Adsorption on NaCl(100)

The adsorption geometries of various benzoic acids on NaCl(100) were obtained by BFGS Hessian update imple-

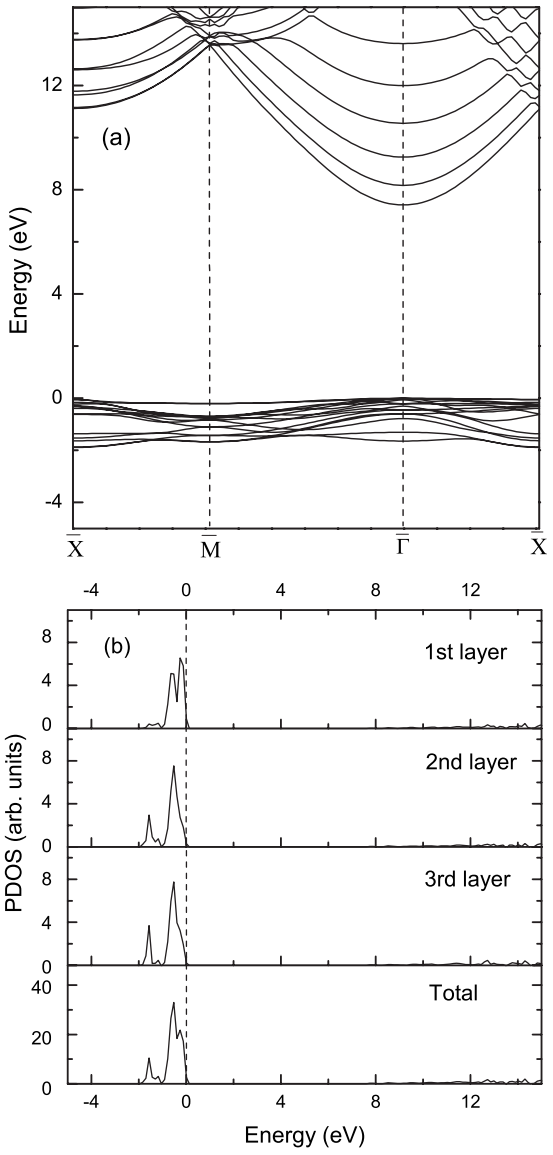

FIG. 4. (a) Band structure and (b) DOS of a five-layer NaCl(100) slab. The top of the valence band is shifted to energy zero.

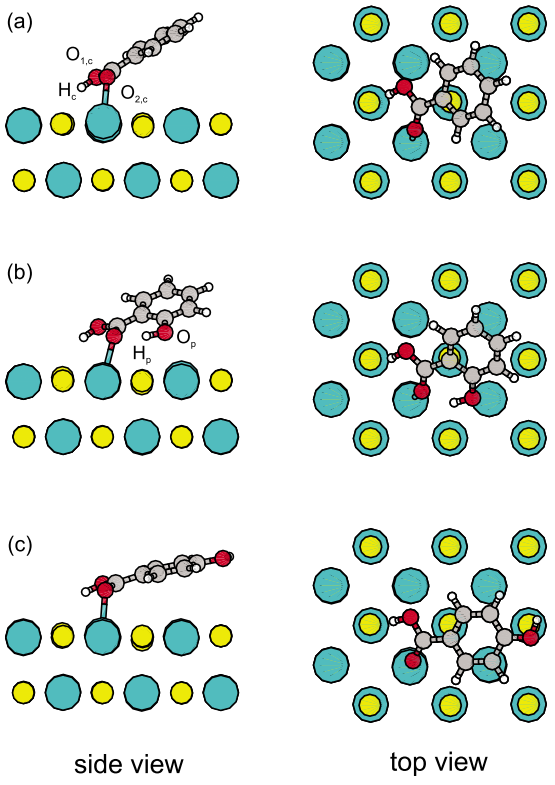

FIG. 5. (Color online) Adsorption geometries of (a) BA, (b) SA, and (c) *p*-SA on the NaCl(100) surface. Only the top two layers of NaCl(100) are shown in the side views. Sodium and chlorine atoms are shown in green (dark gray) and yellow (light gray), whereas oxygen, carbon, and hydrogen atoms of the adsorbates are shown in red (black), smaller gray, and white, respectively.

mented in CRYSTAL06. The molecules were initially placed at different positions on the surface with a vertical separation distance of about 2.5 Å. It is also reasonable to start the optimization from a parallel configuration with a molecule lying flat on the surface, which was suggested by previous experiments.[10,28] The final adsorption geometries for BA, SA, and *p*-SA on NaCl(100) are shown in Fig. 5. The adsorption energy, which is given in Table IV, was calculated by

$$E_{\text{ads}} = E_{\text{M/NaCl}} - E_{\text{NaCl}} - E_{\text{M}}, \tag{5}$$

where $E_{\text{M/NaCl}}$, E_{NaCl}, and E_{M} denote the total energy of the adsorbed system, NaCl(100), and the isolated molecule, respectively. It is necessary to include a basis set superposition error (BSSE) correction for the adsorption energy in all calculations using the Gaussian-type basis set because the adsorption energy is usually overestimated as a consequence of basis set incompleteness. The BSSE corrected adsorption energy calculated using the usual counterpoise scheme is expressed as[37]

$$E_{\text{ads}}^{\text{BSSE}} = E_{\text{ads}} + (E_{\text{NaCl}} - E_{\text{NaCl}\|\text{M}}) + (E_{\text{M}} - E_{\text{M}\|\text{NaCl}}), \tag{6}$$

where $E_{\text{ads}}(E_{\text{NaCl}})$ is the energy of the NaCl(100) surface (adsorbate molecule) at its optimized adsorption geometry, whereas $E_{\text{NaCl}\|\text{M}}(E_{\text{M}\|\text{NaCl}})$ is the energy of NaCl(100) (adsorbate molecule) with optimized geometry including ghost basis functions on the molecule (surface). As shown in Table IV, the BSSE correction to the adsorption energy amounts to about 0.2 eV, which is nearly 30% of the uncorrected adsorption energy. It is clear that all three molecules bind to the surface through the interaction between a surface Na atom and the carboxylic oxygen. For SA, an additional bonding between Na and the phenolic oxygen is present. Moreover, it can also be seen in Fig. 5 that the carboxylic hydrogen points downward to the surface Cl as a result of the interaction between these two atoms. Some representative bond lengths for the adsorption geometries are presented in Table IV. Overall, the bindings between various benzoic acids and NaCl(100) surface are quite weak. The adsorption energy for SA (0.48 eV) is largest among these three molecules because of the additional interaction between phenolic oxygen and surface sodium atoms. It is indeed this additional Na-O interaction that makes the SA tilted, so that the aromatic ring is slightly rotated. The adsorption configurations for BA and *p*-SA are, on the other hand, very similar (see Fig. 5 and the bond lengths given in Table IV), although *p*-SA is more parallel to the surface than BA. It is noteworthy that all molecules still remain planar after adsorption, and the intramolecular structure distortion shown in Table V is very small. This is in agreement with previous experimental data.[10] Nevertheless, the contraction or the expansion of the intramolecular bond lengths reflect how the molecule interacts with the surface. Exemplarily, the expansion of the intramolecular hydrogen bond $O_{2,c}$-H_p is a consequence of the interactions between Na-$O_{2,c}$ as well as Cl-H_p. Additionally, we find that the dissociative adsorption where the carboxylic hydrogen is detached from the molecule is thermodynamically unfavorable compared to molecular adsorption.

TABLE IV. Adsorption energies, representative bond lengths, and charge transfer to the adsorbates for adsorption on NaCl(100). The subscripts *c* and *p* denote atoms in carboxylic and phenolic groups, respectively (see Fig. 5).

	Adsorption energy (eV)		Bond lengths *d* (Å)					Charge (*e*)
	E_{ads}	$E_{\text{ads}}^{\text{BSSE}}$	Na-$O_{1,c}$	Na-$O_{2,c}$	Na-O_p	Cl-H_c	Cl-H_p	
BA	−0.60	−0.43	2.74	2.37		2.18		0.021
SA	−0.70	−0.48	3.25	2.37	2.50	2.31	2.97	0.001
p-SA	−0.61	−0.41	2.74	2.37		2.44		0.016

TABLE V. Changes of intramolecular bond lengths Δd (in %) for various benzoic acids adsorbed on NaCl(100).

	Carboxyl			Phenol		
	$C\text{-}O_1$	$C\text{-}O_2$	$O_1\text{-}H$	C-O	O-H	$O_2\text{-}H_p$
BA	0.64	−0.57	1.58			
SA	0.42	−0.84	1.22	0.98	−0.01	1.93
p-SA	0.77	−0.79	1.00	−0.30	0.02	

The charge-density difference map shown in Fig. 6 reveals more details of the bonding between functionalized benzoic acids and NaCl(100). Here we use SA as an example because the nature of the bonding is qualitatively the same for both BA and *p*-SA. In Fig. 6 major electron accumulation can be seen in the region between the carboxylic O atom and the surface Na atom. Yet, most of the electrons forming the bond are contributed by the lone-pair electrons from carboxylic oxygen, which makes the bonding character covalent or, more specifically, a dative bond. The charge transfer is evaluated by Mulliken population analysis, as given in Table IV. It shows that there are very small amount of electrons transferred to the benzoic acids after adsorption. Although the partition of electrons based on the Mulliken population is rather arbitrary and basis set dependent, this small charge transfer is still expected in the context of the small intramolecular distortion of these molecules as well as their low binding energies to the surface.

One important aspect missing so far for the adsorption of various benzoic acids on NaCl(100) is the long-range dispersion forces between the π electrons from the molecules and the surface, which unfortunately cannot be described by the semilocal PW91 correlation functional. Indeed this is the primary problem existing in standard DFT when it comes to the adsorption of π-conjugated molecules, where the van der Waals (vdW) interactions could be significant.[38] There were several successful attempts trying to remedy this deficiency, some of which use semiempirical methods,[39] while recently an *ab initio* implementation was proposed by introducing a vdW-DF to standard DFT.[40] With this functional, it was found that although the interaction between phenol and graphite(0001) is, not surprisingly, purely nonlocal and long ranged, the adsorption for phenol on α-Al_2O_3(0001) is predominantly governed by the covalent bonding between the phenolic O atom and a surface Al atom.[41] The vdW contribution for adsorption on alumina is thus secondary yet not negligible. Our preliminary calculation using vdW-DF suggests that the adsorption energy of SA on ideal NaCl increases to about 0.8 eV with the long-range dispersion taken into account.[42] Therefore, the vdW interaction is not predominant because of the covalent bonding similar to that of the O-Al bond for phenol on alumina. Nevertheless, in terms of adsorption geometry, if the vdW interaction is included the benzoic acids would be more parallel to the NaCl(100) surface as a result of the interaction between the π electrons located at the aromatic ring and ionized surface Na atom.

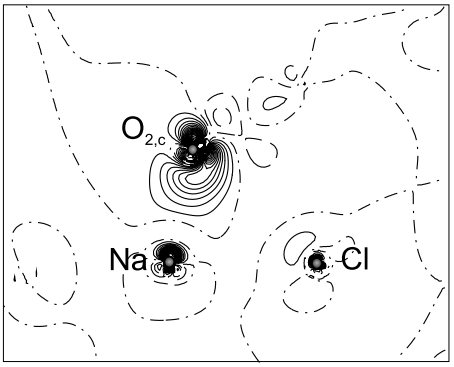

FIG. 6. Change in electron density for Na-O bonding after SA adsorption on NaCl(100). The solid and the dashed lines represent electron accumulation and depletion, respectively. The dashed-dotted line indicates zero. The difference between adjacent lines is $0.015e/\text{bohr}^3$.

The effect of various benzoic acids on the electronic structure of the adsorbed NaCl(100) is illustrated in Fig. 7. It is evident from the band structures that the effective band gap of the adsorbed surface is now dependent on the distance between the HOMO and the LUMO of the adsorbate. The calculated band gaps are 5.68, 4.86, and 5.16 eV for BA, SA, and *p*-SA adsorbed NaCl(100), respectively. Another eminent feature shown in the projected DOS plots in Fig. 7 is the broadening of splitting of some occupied molecular orbitals of the adsorbate. In order to get a closer view of the electronic properties, a blowup of the DOS projected on SA after its adsorption on NaCl(100) is given in Fig. 8, along with the molecular orbital levels of an isolated SA molecule for comparison. It is evident that band splitting occurs for the HOMO−1, HOMO−2, and HOMO−3 of the adsorbate, while the HOMO−2 exhibits a large band broadening. As clearly seen from the electron-density isosurfaces, the electrons of the HOMO−2 and HOMO−3 are mainly located at the in-plane p_{xy} and out-of-plane p_z orbitals of the carboxylic O atom, respectively. Apart from the appreciable π electron density of the benzene ring, the HOMO−1 also exhibits a small but non-negligible electron density on the carboxylic O atom. Therefore, it is the covalent bonding between the carboxylic O atom and the surface Na atom that gives rise to the band broadening and splitting of the adsorbate level, since the HOMO−2, HOMO−3, and to some extent the HOMO −1 should be responsible for the bonding. Similar features have been found when 4-hydroxy-thiophenol was adsorbed on NaCl(100).[43] Generally, the energy level of an adsorbate may experience shifts and broadening when interacting with a broadband. When it couples to the narrow bands, bonding

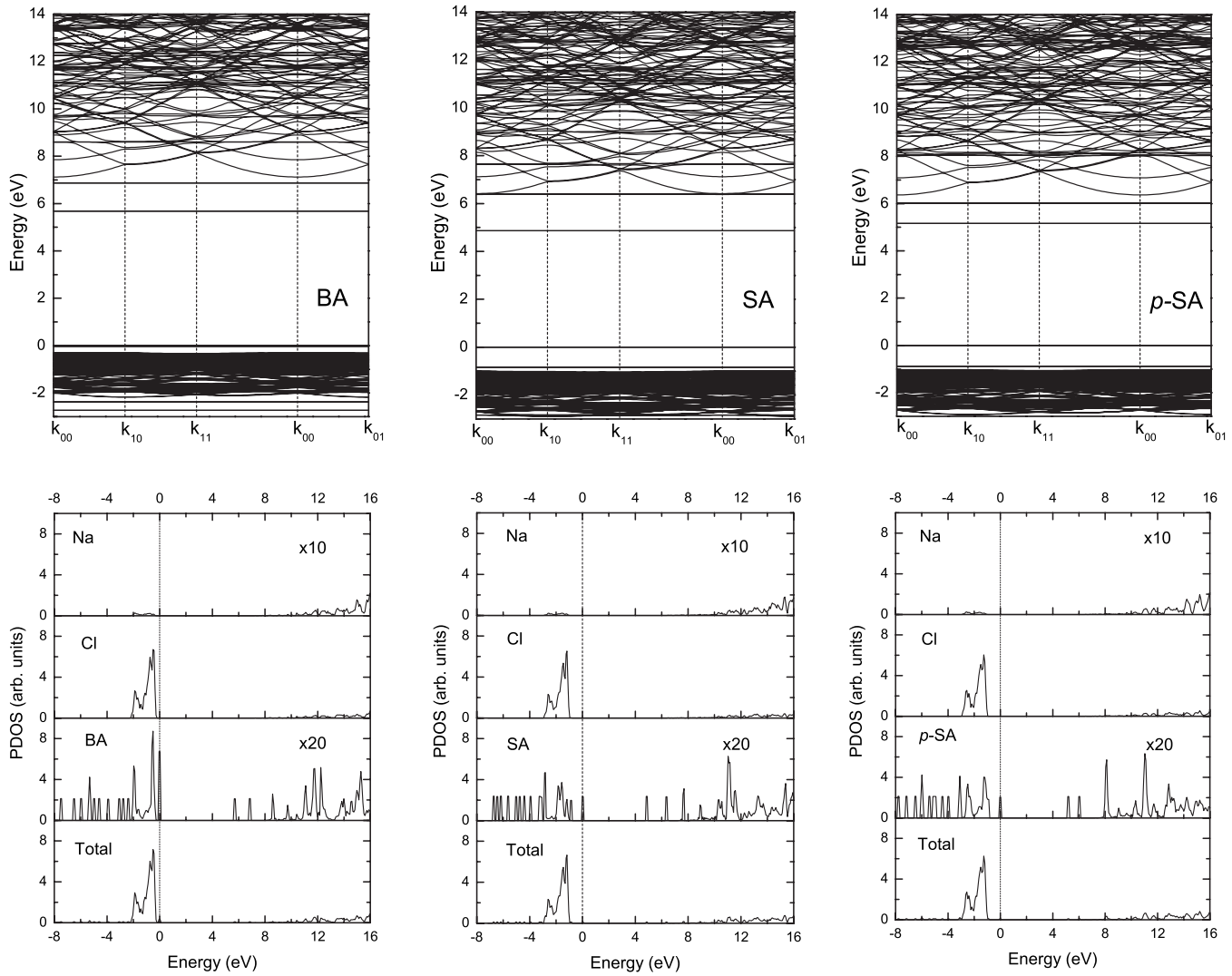

FIG. 7. Band structures (top row) and PDOS (bottom row) of BA, SA, and *p*-SA adsorbed on NaCl(100). The respective HOMOs are set to energy zero.

and antibonding states appear as a result of hybridization. This is exactly what is observed in Fig. 8. For example, an antibonding state appears 0.1 eV above the HOMO−2 of the isolated SA molecule, whereas the corresponding bonding state is 0.2 eV below the HOMO−2. In addition, as both the bonding and antibonding states are still fully occupied, binding between the benzoic acids and NaCl(100) surface is thus quite weak.

We also compared the calculated band structures to earlier experiments.[10,28] There is somehow inconsistency in the band alignment between the HOMO of the adsorbate and the valence-band maximum (Γ_{15}) of NaCl(100). The previous UPS measurements positioned the HOMOs of SA and *p*-SA 0.1 and 0.3 eV above the Γ_{15} point, respectively. For BA, its HOMO is located 0.61 eV below the Γ_{15} point. However, as shown in Fig. 7, DFT calculations with PW1PW functional predict the HOMOs of BA, SA, and *p*-SA 0.3, 1.0, and 1.1 eV above the Γ_{15} point, as a consequence of the resonance effect between HOMO−2 of the adsorbate and the surface valence band. For this kind of weakly bound system the molecular orbitals of the adsorbate do not change much from its isolated state although there is small energy shift and splitting. Thus the band alignment issue could be a signal of some missing interactions in the DFT calculations. Indeed, the lack of vdW interaction in our calculations might be the cause that misaligns the HOMO with respect to the Γ_{15} point. If the interaction between the π electron and the surface is taken into account, we can roughly align HOMO or HOMO−1 to the Γ_{15} point because electrons in HOMO and HOMO−1 are mainly located at the aromatic ring (see Fig. 8). As a result, this gives a better agreement with the experimental findings, but the real picture behind the band alignment is much more complicated and cannot be achieved until vdW interaction is implemented in the calculation. Nevertheless, the overall electronic properties predicted here are still valid as the Na-O interaction is predominant for adsorption of benzoic acids on NaCl(100).

IV. ADSORPTION AT SURFACE VACANCIES

In this section we discuss the influence of NaCl(100) surface vacancies on the adsorption of benzoic acids. The F_s

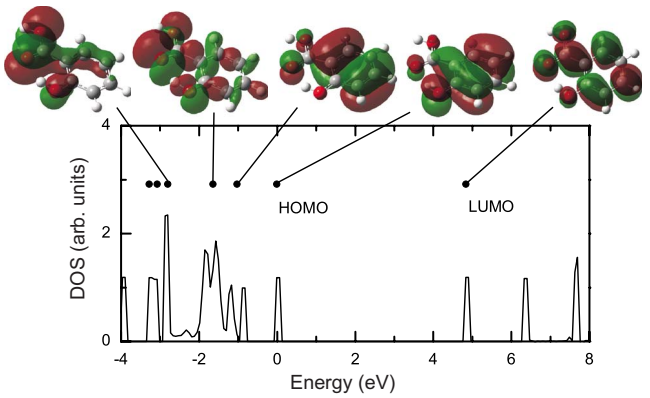

FIG. 8. (Color online) Projected DOS on SA after adsorption on NaCl(100). The solid dots correspond to the energy levels of an isolated SA molecule at the adsorption geometry for direct comparison. The electron-density isosurfaces of five frontier orbitals are also given. Zero energy is at the HOMO.

center, a surface anion vacancy, is one of the most common surface defects in ionic insulators. Therefore we concentrate on the adsorption at the F_s center in this study.

A. NaCl(100) F_s center

The neutral F_s center was created from the five-layer-thick NaCl(100) slab with a (3×3) unit cell used in the last section, which is sufficiently large to exclude defect-defect interactions. One Cl atom was removed from the surface to form the anion vacancy. Therefore, one unpaired electron is left in the vacancy center whose electronic wave function is expanded by the same basis set used for Cl atoms to have an accurate description of the vacancy. Compared to the perfect NaCl(100) surface, the geometry relaxation shows that the four Na atoms closest to the F_s center in the top layer shift toward the vacancy by 0.021 Å, and the displacement of the Na atom beneath the F_s center in the second layer toward the defect is 0.29 Å. The four second shell Cl neighbors in the top layer also show displacements of 0.021 Å toward the vacancy. It is noteworthy that the inward relaxation of the nearest cations around the cavity is quite different from what has been found for other wide-band-gap ionic insulators such as MgO and LiF.[44–46] To understand this discrepancy, geometry relaxations have been calculated within the HF and DFT GGA theories, respectively. While the HF theory also predicts an inward displacement of the surface neighboring Na atoms of 0.15 Å, the PW91 functional, however, shows an outward relaxation of 0.002 Å. It is well known that DFT tends to delocalize the electrons, whereas the HF favors more electron localization. The larger degree of delocalization of the unpaired electron gives rise to an effective positive electrostatic potential at the vacancy, which slightly pushes away the neighboring Na atoms. Moreover, if we remove the ghost basis function at the vacancy and add a diffuse function to the neighboring Na atoms for an adequate description of the unpaired electron, it turns out that an outward relaxation can also be achieved with the hybrid PW1PW functional. Despite the ambiguities of the relaxation behavior, the geometry perturbation induced by the F_s center is very small overall.

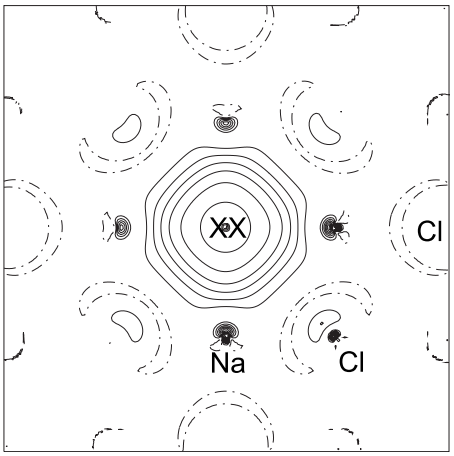

FIG. 9. Electron-spin density with F_s centers on NaCl(100) in the (100) plane. *XX* represents the anion vacancy. The lines are drawn in intervals of $0.01e/\text{bohr}^3$. The solid, dashed, and dotted-dashed lines indicate positive, negative, and zero values, respectively.

The formation energy E_f of an F_s center as the energy required to extract a Cl atom is given by

$$E_f = E_d + E_{\text{Cl}} - E_{\text{NaCl(100)}}, \tag{7}$$

where E_d and E_{Cl} are the total energies of the NaCl(100) with an F_s center and the atomic energy of an isolated Cl atom, respectively. The computed E_f for an anion vacancy is 5.79 eV at the HF level, while PW1PW gives a higher formation energy of 6.47 eV. Nevertheless, these values are in agreement with other theoretical studies.[47,48]

As shown in the spin-density map in Fig. 9, the unpaired electron is well localized in the vacancy center. The trapping is stabilized by the Madelung potential and the effective positive charge on the vacancy. The calculation with the PW1PW functional showed a spin charge of $0.786e$ for the "ghost" vacancy atom (*XX*). The rest of the spin density is spread over the nearest Na ions. The unpaired electron in the vacancy center also introduces singly occupied state in the band gap of NaCl(100). This new electron level lies 2.4 eV below the bottom of the conduction band, which is comparable to earlier EELS results.[10,49]

B. Adsorption at the F_s center

The optimized adsorption geometries of various benzoic acids at NaCl(100) F_s center are given in Fig. 10. The ghost atom was kept fixed during the relaxation. It is evident that all molecules bind to the surface via the interaction between O and Na atoms. For BA and *p*-SA, one carboxylic O atom forms a bond with surface Na, while the other carboxylic O atom binds to the surface in a bridging configuration across two Na atoms. Similar to the adsorption on NaCl(100), there is an additional bonding for the adsorption of SA through the interaction between the phenolic O and the surface Na, which makes its binding energy the largest of all three, as shown in Table VI. The BSSE corrected values are not included in Table VI as BSSE correction gives rise to a large

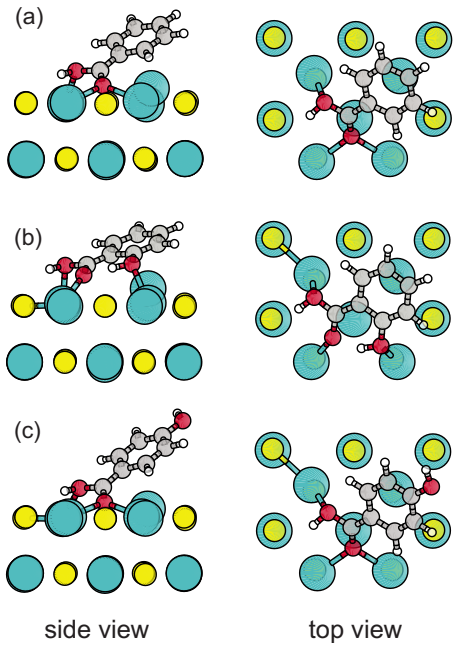

FIG. 10. (Color online) Adsorption geometries of (a) BA, (b) SA, and (c) *p*-SA at an NaCl(100) F_s center. The color scheme is the same as in Fig. 5.

degree of overcorrection in the interaction energy due to the presence of the ghost basis function at the vacancy center. Alternatively, single point energy calculations at the previously optimized structures were performed without the ghost atom, so that the counterpoise scheme can be applied. An additional diffuse function was added to the neighboring Na atoms around the vacancy to give an equivalent description of the F_s center. The basis set for the adsorbate molecule was also improved with the 6-311G(d,p) basis set. For SA, this results in an adsorption energy of 1.39 eV after BSSE correction, which agrees well with our calculations based on the plane-wave basis set. This implies that the real binding energy should be smaller than the values in Table VI by about 0.6 eV. It is evident that the adsorption energies at the vacancy site are much higher than those on the ideal NaCl(100) surface. The increased adsorption energy is partly contributed by the stronger Na-O interactions, which is accompanied by a smaller Na-O bond lengths (see Table VI) compared to the values on the flat NaCl(100) surface. This stronger interaction can be also seen in the intramolecular

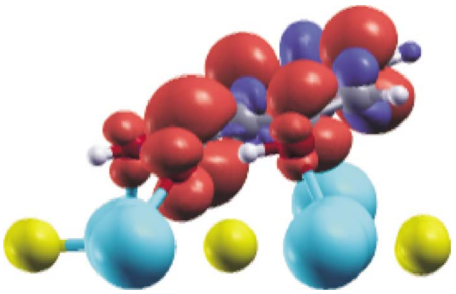

FIG. 11. (Color online) Electron-spin density $\rho^{\alpha\text{-}\beta}$ isosurface for adsorption of SA at the NaCl(100) F_s center. The isovalue is $0.002e/\text{bohr}^3$.

distortion of the molecules, as shown in Table VII. The expansions of the C-O bonds in both carboxylic and phenolic groups are much larger compared to the intramolecular distortions on NaCl(100) without defects (Table V). Nonetheless, the calculation suggests that dissociative adsorption energy of benzoic acids at the F_s center is higher by about 0.6 eV than in molecular adsorption. This is different from the fact that dissociative adsorption of water at the surface color center is energetically favored.[10,14,16] Earlier experiments also revealed that SA is intact after adsorption at F_s centers on NaCl(100),[10] which agrees with our calculations.

In Fig. 11 the spin density $\rho^{\alpha\text{-}\beta}$ for adsorption of SA at F_s is illustrated. It is clear that most of the spin density is now transferred to the carboxylic group and the aromatic ring. This is also evidenced in Fig. 10: the ghost atom is very close to the carboxylic group of the molecules after adsorption. As a consequence, the surface Na^+ ion is attracted by the increased electron density delocalized on the aromatic ring and shows a small displacement toward the molecule, as can be seen in Fig. 10. Such interaction further strengthens the binding.

While the vdW interaction is relatively important for the weakly bound system, it is of less importance in the adsorption at the F_s center due to the larger binding energy. The anion vacancy turns out to be chemically quite reactive, which leads to chemisorption of benzoic acids rather than to physisorption. The net charges on the molecules after adsorption at F_s centers are much higher than the charges transferred from the ideal surface. The gained charges mainly stem from the unpaired electron which is trapped in the vacancy center prior to adsorption.

The electronic properties of the adsorbed system can be revealed by the DOS projected onto the adsorbate. Figure 12

TABLE VI. Adsorption energies, representative bond lengths and spin density $\rho^{\alpha\text{-}\beta}$ of the adsorbates for adsorption at an NaCl(100) F_s center. The BSSE corrected adsorption energy for SA is given in parentheses. The subscripts follow the convention in Fig. 5.

	E_{ads} (eV)	Bond lengths d (Å)				Spin density (e)
		Na-$O_{1,c}$	Na_1-$O_{2,c}$	Na_2-$O_{2,c}$	Na-O_p	
BA	−1.98	2.25	2.32	2.36	0.992	
SA	−2.03 (−1.39)	2.31	2.19		2.28	1.000
p-SA	−1.79	2.24	2.32	2.32		0.995

TABLE VII. Changes of intramolecular bond lengths Δd (in %) for various benzoic acids adsorbed at the NaCl(100) F_s center.

	Carboxyl			Phenol		
	$C\text{-}O_1$	$C\text{-}O_2$	$O_1\text{-}H$	C-O	O-H	$O_2\text{-}H_p$
BA	3.2	6.0	0.3			
SA	3.2	4.7	0.5	2.4	1.9	−7.0
p-SA	3.6	6.5	0.3	0.9	0.0	

shows that the LUMO of the SA molecule is now partly occupied due to the transfer of the unpaired electron from the vacancy to the molecule. Consequently, the HOMO and the HOMO−1, which are mainly located at the aromatic ring, are now split, as is clearly visible in Fig. 12. The broadening and splitting of the HOMO−2, similar to what has been observed on ideal NaCl(100), are indications of the interaction between the carboxylic O atom and the surface Na atom. The splitting of the HOMO, the HOMO−1, and other occupied molecular orbitals shown in Fig. 12 suggests that the electronic properties of the organic molecules are largely altered by spin-density transfer. The HOMO-LUMO separation for SA is reduced to 3.26 eV from the original value of 4.79 eV as a result of the down shift of the partly occupied LUMO. The band gaps for the α spin state, taken as the distance from the LUMO of the adsorbate molecule to the bottom of the conduction band, are 2.72, 2.48, and 2.28 eV for adsorption of BA, SA, and *p*-SA, respectively. Thus it turns out that the presence of an F_s center could narrow the band gap of benzoic acids adsorbed NaCl(100).

V. ADSORPTION ON STEPPED NaCl(100) SURFACES

Steps on NaCl(100) have been found to enhance the adsorption of H_2O (Refs. 14, 17, and 50) and CO_2.[51,52] The electronic structures of ionic materials are also dependent on the properties of the steps on the surfaces.[53] Hence in this section we will present the adsorption energetics and electronic properties of benzoic acids adsorbed on stepped NaCl(100) surface, specifically at the [001]- and the [011]-oriented steps.

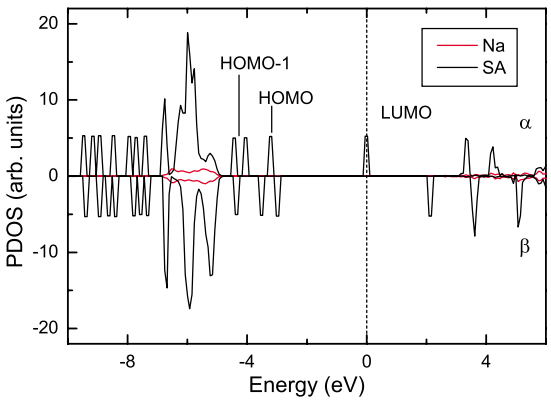

FIG. 12. (Color online) DOS projected onto Na and SA for SA adsorption at F_s.

A. Adsorption at [001]-oriented steps

1. Bare [001]-oriented steps

The [001] step, presented in Fig. 13, is created from a NaCl(301) vicinal surface. The geometry relaxation reveals that the atoms near the step edge tend to move toward their first neighbors, which is illustrated in Fig. 13. Due to symmetry reasons, there is no atomic displacement in the direction parallel to the step edges. From Table VIII, we find that the most undercoordinated atoms, i.e., the edge atoms (Cl_3 and Na_4 in Fig. 13) show the largest displacement. The lower edge atoms (Na_5 and Cl_6) move out of the (100) plane to get closer to their first neighbors, which can be seen as bond contractions in Table VIII. Further, the bond contraction is much stronger when the coordination number (Z) of the atom connected to the edge atom is smaller. For instance, the distance between the edge atom Na_4 and step terrace atom Cl_2 (Z=5) is 2.696 Å, while the lower edge atom Cl_6 (Z=6) is 2.792 Å away from Na_4. Generally the Madelung potential acting on the undercoordinated atoms decreases as the coordination number of their first neighbors decreases. The bond contraction can be regarded as a compensation of the Madelung potential, and thus it becomes larger in the presence of more undercoordinated atoms. However, the overall atomic displacements and bond contractions for the [001] step are still quite limited.

In order to evaluate the formation energy of the [001] step, we start with the ledge energy calculation which can be expressed as

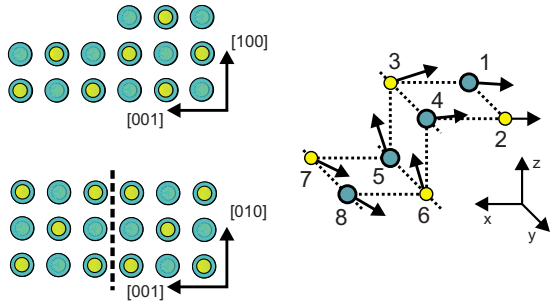

FIG. 13. (Color online) Slab model (left) and geometric relaxation (right) of [001] steps on NaCl(100). Only the [001] step and two underlying NaCl(100) layers are shown. The arrows represent the directions of the atomic displacements. The yellow (light gray) and green (dark gray) circles on the right denote Na and Cl atoms, respectively.

TABLE VIII. Geometric relaxation of the atoms at the [001] step edge site. The subscripts of the atoms are the same as in Fig. 13. The color scheme follows the convention as in Fig. 5.

	Displacement (Å)	
	Δx	Δz
Na_1	−0.11	−0.03
Cl_2	−0.12	0.00
Cl_3	−0.20	0.14
Na_4	−0.26	0.10
Na_5	0.08	0.15
Cl_6	0.07	0.13
Cl_7	−0.01	−0.08
Na_8	−0.02	−0.14
	Changes in interatomic distances	
	Δd (Å)	Δd (%)
Na_1-Cl_3	−0.14	−5.1
Cl_2-Na_4	−0.16	−3.7
Cl_3-Na_5	−0.05	−1.7
Na_4-Cl_6	−0.01	−0.5
Na_5-Cl_7	−0.05	−1.9
Cl_6-Na_8	−0.05	−1.6

$$E_{\text{ledge}} = \frac{E_{\text{step}} - nE_{\text{bulk}} - 2\gamma A}{mL}, \tag{8}$$

where E_{step} is the total energy of the stepped slab which includes n formula units of NaCl. γ, A, and L represent the surface energy of NaCl(100), the surface area, and the step length, respectively. The factor m, accounting for the number of ledges in the unit cell, is 4 for the [001] step. The calculated ledge energy is 67 meV/Å for the rigid stepped surface. Geometric relaxation further decreases the ledge energy to 51 meV/Å. It should be borne in mind that the ledge energy consists of the step energy, which is required to form the step, and the step-step interaction which depends on the separation of the steps.[35,54] Nonetheless, the actual step energy should be slightly lower than the ledge energy since the interstep interaction only has a small contribution to the ledge energy.[35]

To conclude the introduction to the [001] step, the electronic properties of the stepped surface was investigated. The band structure of the relaxed stepped surface (not shown) is very close to that of the flat surface. Indeed, the small perturbations of Madelung potentials around the step site are effectively compensated through geometric relaxation. The computed band gap of the [001] stepped NaCl(100) surface is 7.46 eV, which is just marginally larger than that of the flat NaCl(100) surface, in agreement with experiments.[52]

2. Adsorption at [001] steps

We show here the adsorption of SA as an example, whose most stable adsorption geometry at [001] step is presented in Fig. 14. At the optimized adsorption configuration, the carboxylic O atom of C=O group prefers to bind to the surface at a bridge adsorption site, where it interacts with both the Na atom at the (001) step edge and the Na atom of NaCl(100). Since the step edge atoms are more undercoordinated, the binding of carboxylic O to the step edge Na is stronger than that to the surface Na atom. This can be manifested by the shorter bond length to the step edge Na atom (2.48 Å) than to the surface Na atom (2.61 Å). Likewise the bond length between carboxylic H atom and step edge Cl atom (2.13 Å) is contracted compared to that on the ideal NaCl(100) (see Table IV). In addition, the phenolic O atom also interacts with the surface Na atom with an interatomic separation of 2.75 Å. The charge gain on SA after adsorption is 0.02e according to the Mulliken population analysis. The calculated binding energy including BSSE correction is 0.72 eV, which is 0.24 eV larger than on flat NaCl(100) surface. This affirms that steps are preferred binding sites for molecular adsorption on NaCl surface.

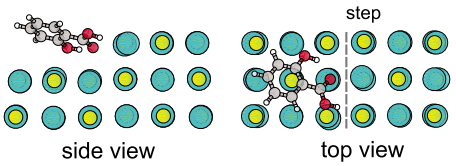

FIG. 14. (Color online) Adsorption geometry of SA at [001] steps on the NaCl(100) surface. The color scheme follows the convention as in Fig. 5.

The electronic structure of benzoic acids adsorbed at the [001] step is, not surprisingly, similar to the adsorption on the flat NaCl(100) surface because of the identical bonding mechanisms. Exemplarily, the band gap obtained for SA adsorbed at the [001] step is 4.75 eV, and the HOMO of SA is positioned 0.88 eV above the VBM of the surface. The influence of vdW interaction on the band alignment is less crucial here because the aromatic ring is now less exposed to the surface. It is reasonable to assert that the adsorption of BA and p-SA qualitatively yields the same trend as on flat NaCl(100), and thus no further calculation was performed.

B. Adsorption at [011]-oriented steps

1. Bare [011] step

Two stoichiometric [011]-step models with different step terrace widths (named S1 and S2) used for the adsorption calculations are presented in Fig. 15. Unlike the [001] step, the edge of the [011] step is either terminated with Cl or Na atom. Such alternating Cl and Na atomic rows induce a net dipole moment along $[01\bar{1}]$ because of the nonzero electrical field between the two neighboring atomic rows.[55–58] This also gives rise to an increase in electrostatic potential when moving from the Cl-terminated step edge to the Na-terminated side. It is clear that the total dipole moment is proportional to the number of the atomic rows along the step direction. As a result, the S2 model is more polar than the S1.

The coordination number of the [011] step edge atoms is 3, making them even more undercoordinated than the step

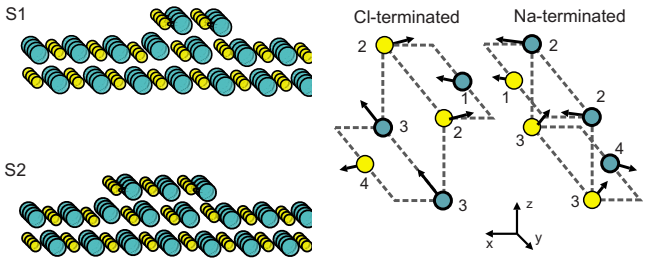

FIG. 15. (Color online) Schematics of relaxed geometries for the [011] step on NaCl(100) with a step width of 4 (S1) and 6 (S2) atomic rows. Only two underlying NaCl(100) layers are shown. The inset shows the displacement directions of the atoms at the step edge site based on the S2 model. The color scheme is the same as in Fig. 5.

edge atoms of the [001] step. The values of atomic charges at the step edge are smaller than those at the step terrace and on the regular surface according to the Mulliken analysis, which corresponds to a lower ionicity at the step edge. Therefore a much larger geometric relaxation is expected, as is presented in Table IX, especially for the edge atoms which have the largest displacements and move toward their nearest neighbors in order to compensate for the reduced Madelung potential. Similar to [001] step, the upper edge atoms tend to retract from step within their layer, in contrast to the lower edge atoms—an effect of higher undercoordination. It is also found that, at the Na-terminated step site, the step edge Na atom shows a larger relaxation than the step edge atom at the Cl-terminated site. Generally both stepped surfaces (S1 and S2) have almost the same geometric relaxation. Yet, the displacements of step edge atoms in the S2 model are slightly larger due to its higher polarity.

TABLE IX. Geometric relaxation of the atoms at the [011] step site. The subscripts of the atoms are illustrated in Fig. 15.

	S1		S2	
	Δx (Å)	Δz (Å)	Δx (Å)	Δz (Å)
Cl terminated				
Na_1	0.22	0.15	0.13	0.14
Cl_2	−0.21	0.12	−0.27	0.16
Na_3	0.26	0.36	0.25	0.41
Cl_4	0.13	−0.12	0.16	−0.10
Na terminated				
Cl_1	−0.07	0.21	0.03	0.21
Na_2	0.42	0.01	0.48	0.01
Cl_3	−0.21	0.28	−0.22	0.32
Na_4	−0.16	−0.16	−0.20	−0.14
	S1		S2	
	Δd (Å)	Δd (%)	Δd (Å)	Δd (%)
Cl terminated				
Na_1-Cl_2	−0.29	−10.1	−0.27	−9.4
Cl_2-Na_3	−0.19	−6.8	−0.20	−7.1
Na_3-Cl_4	−0.05	−1.6	−0.02	−0.8
Na terminated				
Cl_1-Na_2	−0.31	−11.0	−0.29	−10.4
Na_2-Cl_3	−0.20	−7.0	−0.21	−7.5
Cl_3-Na_4	−0.00	−0.1	0.02	0.8

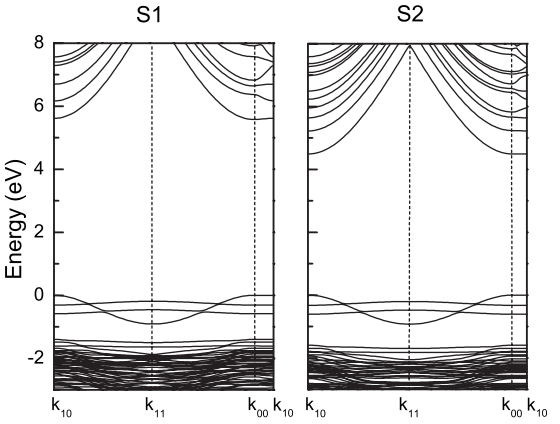

FIG. 16. Band structures of the relaxed [011] stepped NaCl surface constructed by two slab models (S1 and S2). The top of the valence band is aligned to energy zero.

The ledge energy, as calculated from Eq. (8) with $m=2$, is substantially higher than that of the [001] step. The rigid [011] step shows ledge energies of 339 and 406 meV/Å for the S1 and S2, respectively. Relaxation effects significantly lower the ledge energy to 180 and 209 meV/Å, nearly half of the value of the rigid step. The higher ledge energy for the S2 is consistent with its larger atomic displacements of the step edge atoms, as a consequence of the higher polarity along the step direction.

As mentioned in the last section, the electronic structure, specifically the band gap of the stepped surface, is explicitly dependent on the local electronic environment of the step edge atoms. For ionic insulators such as NaCl, the top of the valence band is mostly from Cl p states, and the bottom of the conduction band has partly a contribution from Na Na s states. Thus, the band-gap width is sensitive to the anion-cation interactions. Generally a small Madelung potential corresponds to a decreased gap width. Indeed, we find that the band gap of a rigid [011] step (S1) is merely 2.81 eV. Geometric relaxation enhances the Madelung potential by bond contractions around the step edge atoms, shifting the Na and Cl energy levels toward higher and lower energies, respectively. As a result the band gap recovers to 5.58 eV after relaxation, but it is still about 2 eV smaller than that of the flat surface. The valence-band edge now mainly consists of the $3p$ states from the step edge Cl atoms (cf. Fig. 20). As also seen in Fig. 16, the relaxed S2 stepped surface shows a smaller gap width of 4.52 eV, associated with the upward shift of the step edge Cl $3p$ levels due to the higher polarity in presence of the larger step terrace width. The substantial dispersion of the top of the valence band along $k_{10}-k_{11}$ and

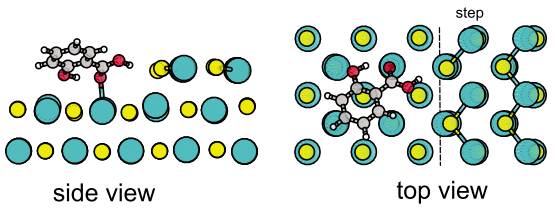

FIG. 17. (Color online) Adsorption geometry of SA at the Cl-terminated side of a [011] step on NaCl(100). The color scheme follows the convention as in Fig. 5.

$k_{10}-k_{00}$ indicates a strong interatomic interaction between the step edge Cl atoms, while the interaction in the direction perpendicular to the step edge is negligible.

To sum up, the reduced Madelung potential acting on the undercoordinated [011] step edge atoms results in much larger relaxation than on a surface with [001] steps. Consequently, the band gap is significantly narrowed due to the shift of the energy levels of step edge atoms toward the midgap.

2. Adsorption at the [011] step

The stoichiometric [011] stepped surface provides two potential adsorption sites for benzoic acids: one at the Cl-terminated step edge and the other on the Na-terminated side. We briefly begin with the study of adsorption at the Cl-terminated site. As an example, the SA adsorbed configuration is presented in Fig. 17 for the S1 step model, where the carboxylic H atom binds to the step edge Cl atom with a bond length of 2.17 Å. Additionally, the carboxylic and phenolic O atoms interact with the (100) terrace Na atoms in the second layer, forming covalent bonds with bond lengths of 2.34 and 2.56 Å, respectively. The computed adsorption energy is −0.80 eV including BSSE correction, which is slightly higher than that at the [001] step. The intramolecular distortion is comparable to that on the flat surface and nearly no charge transfer is observed after adsorption.

The band gap of SA adsorbed at the Cl-terminated step edge of [011] step obtained from the band structure shown in Fig. 18 is 5.01 eV, which is determined by the HOMO-LUMO separation of the adsorbate molecule since the highest occupied state is now essentially the HOMO of SA, as revealed by the PDOS in Fig. 18. In presence of the Na-O bonds, the band splitting and broadening can also be found as a consequence of the interaction between carboxylic O and Na atoms in the second layer, which has also been found as an universal characteristic for adsorption on various NaCl surfaces. It is indeed the resonance between the p_{xy} and p_z states located at the carboxylic group C=O (e.g., HOMO −1, HOMO−2, and HOMO−3) and surface Na states that pins the HOMO of SA as the highest occupied state because the separation of the HOMO and these p states (see Table I) is larger than the upward shift of energy level of the step edge Cl atoms. Although there are splittings and shifts for the molecular orbitals of the adsorbate compared to the isolated molecule, this argument is still valid as the shifts are quite limited. Accordingly, the adsorption of BA and p-SA at the Cl-terminated step edge follows the same way as SA. However, it needs to be pointed out that, due to the small HOMO-(HOMO−1) separation of BA, the band gap for the BA adsorbed at the stepped surface is no longer determined by the HOMO-LUMO gap, since the top of the valence band is now mostly comprised of states from the stepped surface. This is also true for adsorption within the S2 model, where the energy level separation between step edge and surface atoms are even larger than in S1. Nevertheless, the overall band gaps for all three benzoic acids adsorbed at Cl-terminated step edges are still over 4 eV.

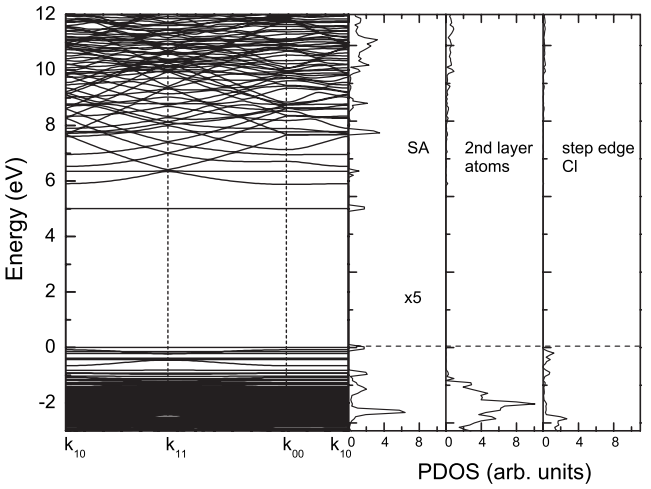

FIG. 18. Band structure (left) and projected DOS (right) of SA adsorbed at the Cl-terminated side of a [011] step on NaCl(100) obtained from the S1 surface model. The highest occupied state is shifted to energy zero.

Now we move the adsorption site from the Cl-terminated to the Na-terminated step edge. The adsorption geometries for various benzoic acids adsorbed at the Na-terminated step edge (S1) are presented in Fig. 19. The adsorption configurations for BA and p-SA are rather similar, where carboxylic O atoms are in interaction with the step edge Na atoms. The adsorption of SA, however, shows a different relaxed configuration, where both carboxylic and phenolic O atoms bind to the step edge. The carboxylic H atom interacts with surface Cl atom, which makes the SA molecule more tilted than BA and p-SA. As shown in Table X, the average Na-O bond length is generally shorter compared to the adsorption on the ideal NaCl(100) surface, indicating stronger bonding between the O atom and the undercoordinated Na atom at the step edge. The adsorption energies are hence much higher than the values on flat NaCl(100). Moreover, the adsorption energy for SA is largest due to the interaction with the phenolic O atom, which is absent for BA and p-SA, following the same trend as on the flat surface. It is clear from Table X that the Na-terminated step edge is a more preferred adsorption site than the Cl-terminated step.

The adsorption configuration does not change with the S2 model. For example, the binding energy for SA adsorbed at Na-terminated step is 1.01 eV, which is slightly higher than that on the S1 surface. Accordingly, the Na-O_p bond length shows a small contraction of 0.02 Å.

However, the electronic structure, specifically the band gap, shows pronounced changes as a function of step width

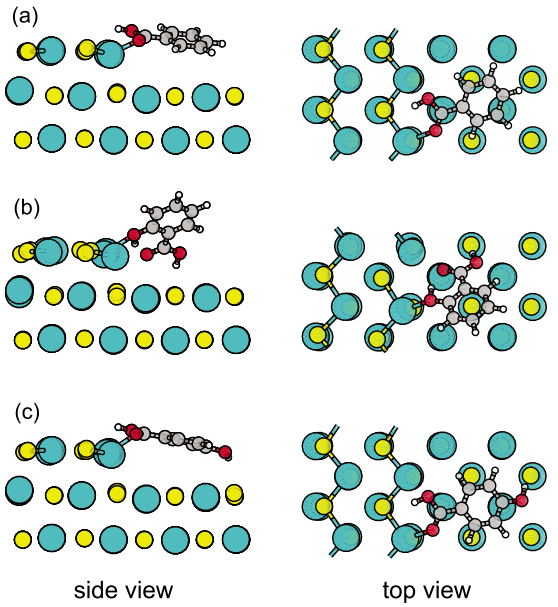

FIG. 19. (Color online) Adsorption geometries of (a) BA, (b) SA, and (c) *p*-SA bound to the Na-terminated step edge of the [011] step on NaCl(100). The color scheme follows the convention as in Fig. 5.

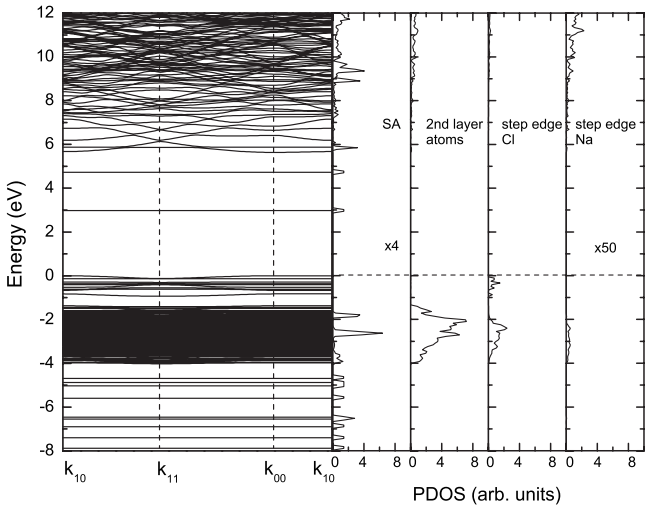

FIG. 20. Band structure (left) and projected DOS (right) of SA bound to the Na-terminated step edge of the [011] step on NaCl(100) obtained from the S1 surface model. The top of the valence band is shifted to energy zero.

for adsorption at the Na-terminated side of [011] steps. We first present the results obtained on the S1 surface. Exemplarily, the band structure and the projected DOS for the adsorption of SA are given in Fig. 20. An obvious feature is the reduced band gap, which only amounts to 2.97 eV, which is nearly 2 eV smaller than on flat NaCl(100). Clearly, the band gap is determined by the separation between the step edge Cl upper valence states and the LUMO state of the adsorbate. By a closer look at the projected DOS, we find that the HOMO−1 and the HOMO−2 of SA are indeed in resonance with the step edge Na states, an apparent indication of the interaction between O atom and step edge Na atom. The step edge Na *s* valence-band center is positioned about 3 eV below the VBM of the stepped surface. As a result of the resonance effect, the HOMO and the LUMO of SA experience a rigid down shift of about 2 eV with respect to the VBM. The same mechanism is also applicable to BA and *p*-SA, leading to effective band gaps of 3.07 and 3.34 eV, respectively.

Interestingly, the adsorption at the Na-terminated step edge using the S2 surface model yields an even smaller gap. The step edge Na *s* valence-band center is about 4 eV below the VBM of the stepped surface. This gives rise to a further rigid shift of the LUMO of about 1 eV toward the valence band compared to the adsorption on the S1 surface due to the resonance effect. As a result, the effective band gap of SA adsorbed at this NaCl stepped surface amounts to 1.80 eV. As mentioned above, this gap reduction with respect to the S1 model arises from the larger step width which enhances the step polarity. This, however, raises the question of how the effective band gap of the adsorbate system is related to the width of the step terrace. In an attempt to elucidate this question, an extended [011] surface model (S3) with a step width of eight atomic rows was also employed for SA adsorption calculations. The resultant band gap is 1.63 eV, which is slightly smaller than that obtained from the S2 surface. It is clear that the band gap is indeed dependent on the surface model employed in the calculation. However, the trend of convergence suggests that the band gap should not experience a pronounced reduction as the step width is further increased. Therefore, we conclude that at [011] stepped surfaces the adsorption of SA could lower the effective band gap of the adsorbed system to about 1.6 eV. In the case of BA and *p*-SA, the band gaps, by a rigid shift of the LUMO referring to the results at the S1 surface, are estimated to be 1.7 and 2.0 eV, respectively.

TABLE X. Adsorption energies, representative bond lengths, and charge transfer to the adsorbates at the Na-terminated step edge for adsorption at the [011] step on NaCl(100) (S1). The subscripts *c* and *p* denote atoms in carboxylic and phenolic groups, respectively.

	Adsorption energy (eV)		Bond lengths *d* (Å)				Charge (*e*)
	E_{ads}	E_{ads}^{BSSE}	Na-$O_{1,c}$	Na-$O_{2,c}$	Cl-H_c	Na-O_p	
BA	−1.09	−0.87	2.47	2.26	2.46		0.009
SA	−1.21	−0.99	3.59	2.40	2.09	2.28	0.046
p-SA	−1.18	−0.91	2.45	2.26	2.57	3.26	0.003

VI. DISCUSSION AND CONCLUSIONS

The adsorption of benzoic acid and its OH-substituted derivatives on the NaCl surface serves as a prototype system for interactions with various organic molecules and wide-band-gap ionic surfaces. As predicted by our *ab initio* calculations with the hybrid exchange-correlation functional PW1PW, it is found that both adsorbate and surface structures have pronounced impact on the adsorption energetics and electronic structures. The adsorbates are bound to the surface primarily through the Na-O bond with a covalent character. Such interaction can be also found on stepped surfaces, as well as at surface vacancy sites. In general, the adsorption of SA has the largest binding energy because of the interaction between phenolic O and Na atoms, which is absent for BA and *p*-SA as shown by the calculations. Indeed, the interaction between a surface Na atom and a carboxylic or phenolic O atom is predominant for adsorption of benzoic acids on NaCl surface, making the vdW interaction of secondary importance for the total adsorption energy. This suggests a general trend for the interaction between ionic surface and organic molecule attached with hydroxyl group where lone-pair electrons are located. In this way a covalent bond forms between a surface cation and an O atom of the hydroxyl group.

The adsorption on the ideal NaCl(100) surface turns out to be quite weak, yielding binding energies of 0.41–0.48 eV for various benzoic acids. For F_s centers and stepped surfaces, the adsorption of benzoic acids is much stronger, in agreement with the general knowledge that F_s center and surface step can enhance adsorption of molecules. The undercoordinated step edge atoms assist the adsorption as a result of a reduced Madelung potential. For example, the binding energy of SA at the Na-terminated step edge of the [011] step increases to 1.01 eV, which is 0.53 eV larger than that on the flat surface. For the F_s center, the unpaired electron trapped in the vacancy center prior to the adsorption transfers to the aromatic ring and to the carboxylic group of the adsorbate, resulting in an additional interaction to the surface cation and thus strengthening the binding. However, different from the dissociative adsorption of water at the F_s center, we find that molecular adsorption of benzoic acid is more stable. This is consistent with previous experiments in which the SA has been found to stay intact at the F_s center.[10] Dissociative adsorption is not favorable on flat NaCl(100) nor on [001]- or [011]-oriented steps. In fact, the intramolecular distortion of the adsorbate is rather small on both flat and stepped surfaces. At the F_s center, however, substantial changes in intramolecular bond lengths have been observed for the adsorbate accompanied by large charge transfer from the vacancy center to the molecule.

Apart from the energetics of adsorption on NaCl surface, a more intriguing feature lies in the electronic structure of the adsorbed system. It is clear from our calculations that the adsorption of benzoic acids on the NaCl surface can effectively decrease the band gap at the surface due to the unoccupied molecular states located in the band gap of pure NaCl. On the ideal NaCl(100) surface, the band gap of the surface with adsorbed molecules reduces to the HOMO-LUMO gap of the adsorbate as a result of the resonance effect mostly between the HOMO−2 of the molecule and surface Na states. Therefore, the effective band gap is essentially correlated with the molecular orbitals of the adsorbate, which can be tuned by the energetic position of the phenolic group. As a consequence, the SA adsorbed NaCl(100) surface gives the smallest band gap of 4.86 eV, while the band gap for the BA adsorbed surface is the largest (5.86 eV). Interestingly, the effective band gap exhibits a dramatic reduction when adsorption occurs at the [011] step site, where the carboxylic O atom binds to the step edge Na atom. The valence-band edge of the [011] step primarily consists of the $3p$ states of the step edge Cl atoms, which are shifted toward the conduction band as a result of the decreased Madelung potential. Subsequently, the effective band gap is determined by the separation between the LUMO and the step edge Cl $3p$ upper valence states. A gap width of only 1.6 eV has been found for SA adsorbed on the [011] steps. It should be mentioned that the electronic structure for adsorption at the F_s center is quite different due to the transfer of the unpaired electron. In any case our results show that the generation of surface defects and adsorbates such as benzoic acids significantly lower the effective band gap of the adsorbate system. The unoccupied electronic states introduced into the original band gap by molecular adsorption are well confined to the surface and therefore of local nature.

Now we are in the position to correlate these results with the contact charging effect between wide-band-gap insulators. The prerequisite of contact charging is mobile charges and the possibility for charge exchange. At room temperature, charge exchange between perfect wide-band-gap insulators such as NaCl and KCl is impossible because the excitation probability is practically zero, leading to no charging effect when they are brought into contact. However, the introduction of unoccupied states from adsorbate can effectively reduce the band gap, so that electrons can excite into the unoccupied state and transfer from one side to the other when two surfaces are in contact until thermal equilibrium is reached. Thus, the efficiency of contact charging is in principle related to the band gap at the surface with or without adsorbed molecules. One can see that although benzoic acids manages to decrease the band gap of the NaCl(100) surface by 2 eV, the overall band gap (about 5 eV) is still too large for thermal electron excitation. This situation can be changed when adsorption occurs at specific step sites. The small band gap of 1.6 eV for SA adsorbed on the Na-terminated [011] step can assist the electron excitation, making charge exchange possible between insulators. The electron excitation energy should be even smaller, since geometric relaxations triggered by exciton formation are not taken into account in our calculations.

Summarizing, we demonstrated how the interplay between defects with the molecular binding allows tailoring of effective band gaps at surfaces of insulators, using the specific example of benzoic acids on the NaCl(100) surface with steps, kinks and color centers. This can lead not only to

enhanced electron transfer like in contact charging, but also to selective chemical reactivity in presence of other molecules. Although it is clear from this investigation that we need a much more systematic understanding of the underlying properties in order to use this effect routinely, it opens interesting perspectives toward potential applications.

ACKNOWLEDGMENTS

The calculations were performed on the CLUH clusters at RRZN Leibniz Universität Hannover and Complex HICE at HLRN-II. Financial support by K+S AG is gratefully acknowledged.

*pfnuer@fkp.uni-hannover.de

[1] D. M. Roessler and W. C. Walker, Phys. Rev. **166**, 599 (1968).
[2] J. Bandet-Faure and L. Touzillier, Surf. Sci. **43**, 183 (1974).
[3] T. R. Pian, N. H. Tolk, M. M. Traum, J. Kraus, and W. E. Collins, Surf. Sci. **129**, 573 (1983).
[4] B. Crone, A. Dodabalapur, Y. Y. Lin, R. W. Filas, Z. Bao, A. LaDuca, R. Sarpeshkar, H. E. Katz, and W. Li, Nature (London) **403**, 521 (2000).
[5] J. H. Burroughes, D. D. C. Bradley, A. R. Brown, R. N. Marks, K. Mackay, R. H. Friend, P. L. Burns, and A. B. Holmes, Nature (London) **347**, 539 (1990).
[6] D. Bloor, Nature (London) **356**, 19 (1992).
[7] C. D. Dimitrakopoulos and P. R. L. Malenfant, Adv. Mater. **14**, 99 (2002).
[8] A. L. Briseno, S. C. B. Mannsfeld, M. M. Ling, S. H. Liu, R. J. Tseng, C. Reese, M. E. Roberts, Y. Yang, F. Wudl, and Z. N. Bao, Nature (London) **444**, 913 (2006).
[9] B. A. Jones, A. Facchetti, M. R. Wasielewski, and T. J. Marks, J. Am. Chem. Soc. **129**, 15259 (2007).
[10] U. Malaske, C. Tegenkamp, M. Henzler, and H. Pfnür, Surf. Sci. **408**, 237 (1998).
[11] H. Pfnür, C. Tegenkamp, V. Maslyuk, and T. Bredow, Surf. Sci. **600**, 1664 (2006).
[12] I. Stahl and U. Kleine-Kleffmann, Kunststoffberater **6**, 28 (1994).
[13] X. Q. Gong, A. Selloni, M. Batzill, and U. Diebold, Nature Mater. **5**, 665 (2006).
[14] A. Allouche, J. Phys. Chem. B **102**, 10223 (1998).
[15] J. Zhu, J. A. Farmer, N. Ruzycki, L. Xu, C. T. Campbell, and G. Henkelman, J. Am. Chem. Soc. **130**, 2314 (2008).
[16] S. Folsch and M. Henzler, Surf. Sci. **247**, 269 (1991).
[17] B. Ahlswede and K. Jug, Surf. Sci. **439**, 86 (1999).
[18] S. Briquez, S. Picaud, C. Girardet, P. N. M. Hoang, J. Heidberg, and A. Vossberg, J. Chem. Phys. **109**, 6435 (1998).
[19] Y. Yang, S. Meng, and E. G. Wang, Phys. Rev. B **74**, 245409 (2006).
[20] J. M. Park, J. H. Cho, and K. S. Kim, Phys. Rev. B **69**, 233403 (2004).
[21] H. Meyer, P. Entel, and J. Hafner, Surf. Sci. **488**, 177 (2001).
[22] R. Dovesi *et al.*, CRYSTAL06, University of Torino, Torino, 2006.
[23] T. Bredow and A. R. Gerson, Phys. Rev. B **61**, 5194 (2000).
[24] J. P. Perdew and Y. Wang, Phys. Rev. B **45**, 13244 (1992).
[25] M. Prencipe, A. Zupan, R. Dovesi, E. Apra, and V. R. Saunders, Phys. Rev. B **51**, 3391 (1995).
[26] G. Bruno and L. Randaccio, Acta Crystallogr., Sect. B: Struct. Crystallogr. Cryst. Chem. **36**, 1711 (1980).
[27] M. Sundaralingam and L. H. Jensen, Acta Crystallogr. **18**, 1053 (1965).
[28] C. Tegenkamp and H. Pfnür, Phys. Chem. Chem. Phys. **4**, 2653 (2002).
[29] A. D. Becke, J. Chem. Phys. **98**, 1372 (1993).
[30] D. R. Lide, *CRC Handbook of Chemistry and Physics*, 87th ed. (CRC, Boca Raton, FL, 2006).
[31] B. J. Marshall and Cr. Cleaveli, J. Phys. Chem. Solids **30**, 1905 (1969).
[32] N. O. Lipari and A. B. Kunz, Phys. Rev. B **3**, 491 (1971).
[33] P. K. de Boer and R. A. de Groot, Phys. Lett. A **256**, 227 (1999).
[34] R. Dovesi, B. Civalleri, R. Orlando, C. Roetti, and V. Saunders, *Ab Initio Quantum Simulation in Solid State Chemistry 1*, Reviews in Computational Chemistry Vol. 21 (John Wiley & Sons, Inc., New York, 2005).
[35] B. Li, A. Michaelides, and M. Scheffler, Phys. Rev. B **76**, 075401 (2007).
[36] J. Vogt and H. Weiss, Surf. Sci. **491**, 155 (2001).
[37] S. F. Boys and F. Bernardi, Mol. Phys. **19**, 553 (1970).
[38] P. Sony, P. Puschnig, D. Nabok, and C. Ambrosch-Draxl, Phys. Rev. Lett. **99**, 176401 (2007).
[39] X. Wu, M. C. Vargas, S. Nayak, V. Lotrich, and G. Scoles, J. Chem. Phys. **115**, 8748 (2001).
[40] M. Dion, H. Rydberg, E. Schroder, D. C. Langreth, and B. I. Lundqvist, Phys. Rev. Lett. **92**, 246401 (2004).
[41] S. D. Chakarova-Kack, O. Borck, E. Schroder, and B. I. Lundqvist, Phys. Rev. B **74**, 155402 (2006).
[42] W. Chen, C. Tegenkamp, and H. Pfnür (unpublished).
[43] C. Tegenkamp and H. Pfnür, J. Chem. Phys. **118**, 7578 (2003).
[44] G. Mallia, R. Orlando, C. Roetti, P. Ugliengo, and R. Dovesi, Phys. Rev. B **63**, 235102 (2001).
[45] A. Ferrari and G. Pacchioni, J. Phys. Chem. **99**, 17010 (1995).
[46] C. Gilbert, R. Smith, and S. Kenny, Nucl. Instrum. Methods Phys. Res. B **255**, 166 (2007).
[47] V. E. Puchin, A. L. Shluger, and N. Itoh, Phys. Rev. B **47**, 10760 (1993).
[48] W. C. Mackrodt and R. F. Stewart, J. Phys. C **10**, 1431 (1977).
[49] V. Zielasek, T. Hildebrandt, and M. Henzler, Phys. Rev. B **62**, 2912 (2000).
[50] Q. Dai, J. Hu, and M. Salmeron, J. Phys. Chem. B **101**, 1994 (1997).
[51] C. Tegenkamp, W. Ernst, M. Eichmann, and H. Pfnür, Surf. Sci. **466**, 41 (2000).
[52] C. Tegenkamp, J. Phys.: Condens. Matter **21**, 013002 (2009).
[53] J. Goniakowski and C. Noguera, Surf. Sci. **340**, 191 (1995).
[54] E. D. Williams, Surf. Sci. **299-300**, 502 (1994).
[55] C. Noguera, J. Phys.: Condens. Matter **12**, R367 (2000).
[56] G. Geneste, J. Morillo, F. Finocchi, and M. Hayoun, Surf. Sci. **601**, 5616 (2007).
[57] J. Goniakowski, F. Finocchi, and C. Noguera, Rep. Prog. Phys. **71**, 016501 (2008).
[58] A. Pojani, F. Finocchi, J. Goniakowski, and C. Noguera, Surf. Sci. **387**, 354 (1997).